Computers in Biology and Medicine 43 (2013) 1815–1826

Contents lists available at ScienceDirect

Computers in Biology and Medicine

journal homepage: www.elsevier.com/locate/cbm

Hybrid fusion of linear, non-linear and spectral models for the dynamic modeling of sEMG and skeletal muscle force: An application to upper extremity amputation

Chandrasekhar Potluri *, Madhavi Anugolu, Marco P. Schoen, D. Subbaram Naidu, Alex Urfer, Steve Chiu

Measurement and Control Engineering Research Center, Idaho State University, Pocatello, ID 83209, USA

ARTICLE INFO

Article history:
Received 19 February 2013
Accepted 31 August 2013

Keywords:
Data fusion
Muscle force estimation based on sEMG
Spectral models
Wavelets
Wiener–Hammerstein.

ABSTRACT

Estimating skeletal muscle (finger) forces using surface Electromyography (sEMG) signals poses many challenges. In general, the sEMG measurements are based on single sensor data. In this paper, two novel hybrid fusion techniques for estimating the skeletal muscle force from the sEMG array sensors are proposed. The sEMG signals are pre-processed using five different filters: Butterworth, Chebychev Type II, Exponential, Half-Gaussian and Wavelet transforms. Dynamic models are extracted from the acquired data using Nonlinear Wiener Hammerstein (NLWH) models and Spectral Analysis Frequency Dependent Resolution (SPAFDR) models based system identification techniques. A detailed comparison is provided for the proposed filters and models using 18 healthy subjects. Wavelet transforms give higher mean correlation of 72.6 ± 1.7 (mean $\pm$ SD) and 70.4 ± 1.5 (mean $\pm$ SD) for NLWH and SPAFDR models, respectively, when compared to the other filters used in this work. Experimental verification of the fusion based hybrid models with wavelet transform shows a 96% mean correlation and 3.9% mean relative error with a standard deviation of ± 1.3 and ± 0.9 respectively between the overall hybrid fusion algorithm estimated and the actual force for 18 test subjects' k-fold cross validation data.

1. Introduction

According to information provided by the National Limb Loss Information Center [1], the number of people with missing limbs in the United States is over 1.7 million. The wars in Iraq and Afghanistan substantially increased the number of amputees. In recent years, there has been much progress in developing prostheses for individuals who have sustained hand amputation. The research in the field of prostheses was initiated by the United States National Academy of Sciences [2]. To date, there are multiple types of hand prostheses available. However, there are no prosthetic devices available at an affordable cost and with tactile or proprioceptive feedback for grasping [3]. Rehabilitation robotics is human-centered and deals with a different set of requirements such as mechanical compliance, flexibility, adaptability towards the user, gentleness, safety, humanoid appearance and behavior [4]. Human-centered robotics requires a natural means of communication [5]. In the case of prosthetic devices, one way of interface between the human arm and prostheses is the surface Electromyography (sEMG) itself. sEMG signals are more convenient to use than neuromuscular activation based signals because of their non-invasive feature [6] and because they do not require any bulky mechanism to capture the corresponding signals. The sEMG signals correlate to the electrical emitted activity (voltages) ranging from -5 to $+5$ (mV) generated when muscles contract [7]. sEMG has many applications in many fields other than prostheses. sEMG signal analysis can be found in the field of biofeedback [8], sports [9], and clinical decision making [10].

The sEMG signal amplitude depends on different movements and force levels and varies from person to person. One of the major problems in capturing sEMG signals is cross-talk i.e., the signals propagated from adjacent muscle groups or resulting from firing of different motor units simultaneously during the muscle contraction [11]. Muscle fatigue increases the recruitment of more motor units and decreases mean frequency which results in the force generating capacity of the muscles [12,13]. The sEMG signals pass through several layers of tissues before reaching the skin surface [11]

Abbreviations: ADC, Analog to Digital Converter; AIC, Akakie Information Criterion; BIC, Bayesian Information Criterion; Db, Daubechies; DKF, Decentralized Kalman Filter; DWT, Discrete Wavelet Transform; KIC, Kullback Information Criterion; OLMFA, Optimized Linear Model Fusion Algorithm; OE, Output Error Model; PAFA, Probability Analysis based Fusion Algorithm; PCA, Principle Component Analysis; ICA, Independent Component Analysis; sEMG, Surface Electromyography; SPFDR, Spectral Analysis Frequency Dependent Resolution; VWA, Variance Weighted Average; WH, Weiner Hammerstein

* Corresponding author. Tel.: +1 208 705 8649.
E-mail addresses: Potlchan@isu.edu, chandupotluri@gmail.com (C. Potluri).

0010-4825/$ - see front matter © 2013 Elsevier Ltd. All rights reserved.
http://dx.doi.org/10.1016/j.compbiomed.2013.08.023

Nomenclature

A_1	Mother chromosome
A_2	Father chromosome
$B(q)$ and $F(q)$	polynomials
F_f	Fitness function
$G(q)$	Transfer function providing the dynamic relationship
H	Highest number in parameter range
$H(s)$	MISO transfer function
J	Cost function
L	Lowest number in parameter range
$M_1(s), M_2(s)..., M_k(s)$	Spectral models
M_1, M_2 and M_3	Estimated models from the sEMG sensor data $-u_1(t)$, $u_2(t)$and $u_3(t)-$ and the corresponding skeletal muscle force
M_R	Mutation rate
N_{IP}	Population size of generations
N_{PA}	Number of sensors
N_{PM}	Number of parameters to be mutated
R_i	Residual square norm
T_{NP}	Total number of parameters
$U(\omega)$	sEMG converted to frequency domain
$Y(t)$	Skeletal muscle force
$Y(\omega)$	Force converted to frequency domain
$\hat{Y}_f$	Fused force output
$\hat{Y}_i$	Estimated force
b, f	Coefficients
$e(t)$	Error
f, h	Nonlinear functions
g_i	Low-pass filter with impulse response
h_i	High pass filter
i	Corresponding sensor
n	Number of data points
n_k	System delay
nb, nf	Row vectors
os_1, os_2	Off springs
p_i	Order of particular model
$p_1, p_2, \ldots p_N$	Chromosomes
q	Back shift operator
t	Time index
t_o, t_f	Initial and final time
$u_{u_{fi}}$	Unfiltered sEMG signal
u_{fi}	Filtered sEMG signal using wavelets
$w(t), x(t)$	Interval variables
x	Latent driving signal
α	Expected rate of gradual drift
β	Expected rate of sudden shift in the signal
β_{GA}	Random number on the interval [0,1]
ω	Frequency of the signal
λ, υ	Weighing coefficients
$\|EMG\|$	Rectified EMG signal

and, due to the chemical changes in the skin layers, results in the decrease of the electrical voltage to 50% within in a few seconds [14]. The outcome of noise in electrical circuits and electrical fluctuations is one of the causes for the stochastic nature of the EMG signal; causing additional difficulty in studying it [15]. The sEMG signal characteristics change with time due to fatigue. The sEMG signal is amplitude modulated and time dependent; it is therefore spatially and temporally frequency encoded [16]. All the above mentioned factors make it rather complex to decipher the content of the EMG signal. So, to retain the useful content of the sEMG signal, external noise needs to be filtered. A detailed study was conducted based on the different available filtering techniques using Butterworth, Chebyshev Type II, Bayesian Exponential, and Bayesian Half-Gaussian filters [17–20]. In this present research, a Wavelet Transform (WT) that utilizes the Daubechies 44 (Db 44) mother wavelet is examined for the sEMG/skeletal muscle force modeling and compared to the above listed filters used by the authors in their previous work.

In the field of biomechanics, an important consideration is to obtain insight into the muscle force magnitude [21]. Such information can be used to extract the joint loading information. According to [22], force estimation based on sEMG measurements is one of the best alternatives to the commercially available force measuring sensors. Several different methodologies were proposed to address the sEMG based skeletal muscle force estimation. A method for force estimation was introduced by combining a motor unit twitch model with motor unit pulse trains obtained from the multi-channel surface electromyogram and artificial neural networks [23,24]. This type of force estimation uses the sEMG signals obtained from the upper arm muscle and elbow joint angular position velocity to predict the relationship between the EMG and the generated force. The EMG-to-torque relationship was narrowed down to a linear least squares problem in which a study of a few estimator processors such as single/multiple-channel un-whitened/whitened/adaptively-whitened were used to classify the EMG-torque relationship [25]. It concludes that the joint torque estimation can be improved with higher fidelity EMG amplitude processing. Another interesting algorithm based on the instrumental variable principle was proposed to obtain the dynamic relationship between the electrical and mechanical activity of the muscle [26]. It states that the least-squares, generalized least-squares and maximum likelihood estimators failed because of the nature of the noise assumptions.

In this present work, a methodology based on the System Identification (SI) technique is investigated to determine the sEMG-Force mathematical relationship. We utilized time domain linear, nonlinear, and frequency domain modeling techniques to analyze the dynamics of the sEMG signals. Results are compared with the above mentioned sEMG-Force estimation techniques. The sEMG measurements are based on single sensor data. Different methods were proposed in acquiring the sEMG data using a single electrode to develop a human computer interface [27,28]. In general, the sEMG signals are acquired by placing a single bipolar electrode on the muscle belly [29] which limits their accuracy. So, for this present work, an array of three sEMG sensors and a Force Sensing Resistor (FSR) are used to acquire the EMG signal and the corresponding skeletal muscle force. While using multiple electrodes, the orientation of the electrodes also plays an important role because of the motor point location approximation. The misalignment of the electrodes leads to the sEMG amplitude reduction [30]. The sEMG sensors are aligned perpendicular to the superficial musculature (flexor digitorum superficialis). The goal of proposing a sensor data fusion method is to improve the accuracy of the skeletal muscle force estimation. In general, data fusion is a process of combining the data sets from different sources to gain more information. It can be achieved in three different ways: Data-level fusion, feature -level fusion, and decision-level fusion. Data level fusion is the combination of data from the sources; feature-level fusion is merging the features of the sources, and decision-level fusion is the combination of the results from the sources. In this work, decision-level fusion is used to combine the data from the three sensors. The information extracted from the three sEMG sensors is fused with a proposed fusion algorithm to improve the skeletal muscle force estimation. The proposed fusion algorithm is developed for an arbitrary number of sensors.

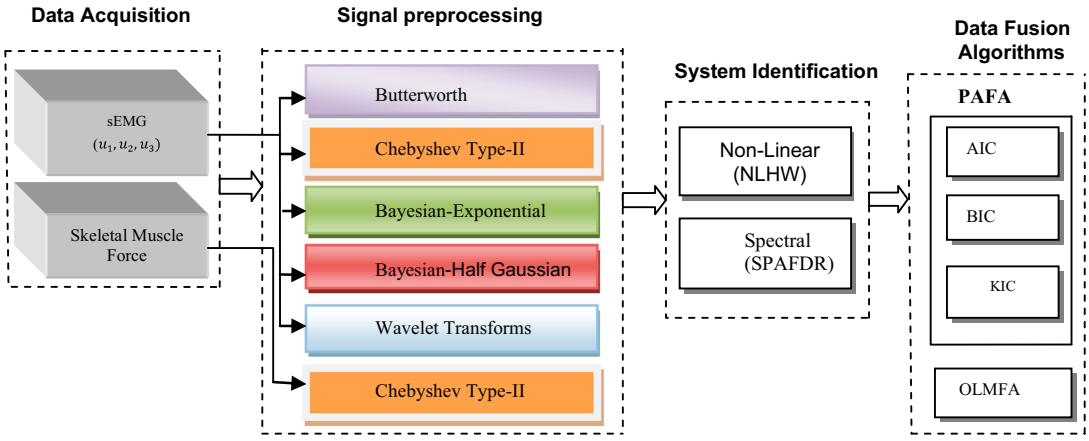

Fig. 1. Block diagram representation of the overall proposed scheme. Data acquisition block represents the acquisition of the sEMG and the skeletal muscle force signals. The signal preprocessing block represents the various filtering techniques used in this work. The System Identification (SI) and the data fusion algorithms represent the SI techniques and the data fusion algorithms employed in this work.

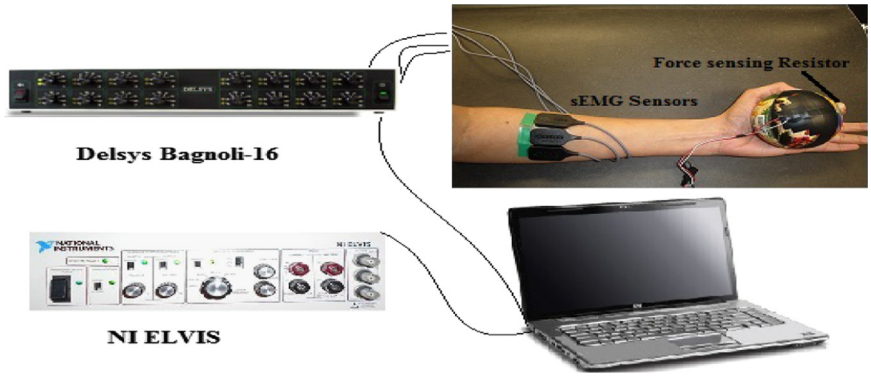

Fig. 2. Experimental design for SEMG data capturing, electrode placement, force sensor and finger positions, (ground electrode on the elbow not shown).

However, for this work the utilized sensor size in relation to the innervation zone including specific motor point location is too large to employ more than three sensors. The fusion-based force shows a better estimation of the skeletal muscle force from the corresponding sEMG signal when compared to single sensor models [31]. In this paper, two different fusion algorithms, one with a simple elitism based Genetic Algorithm (GA) and the other with a probability analysis, are proposed and compared for fusing the sEMG data from three sensors. In addition, this approach is also compared with the existing Variance Weighted Average (VWA) and Decentralized Kalman Filter (DKF) fusion algorithms [32].

The paper is organized as follows. The present section covers the literature review and introduction, and the next section describes the experimental design for acquiring the sEMG and the corresponding skeletal muscle force signals. These are followed by the methodology, fusion algorithms, results and discussion. Some conclusions are provided at the end. Fig. 1 gives an overview of this work.

2. Experimental design

Fig. 2. illustrates the experimental design used for the data acquisition. Experiments were conducted on 18 healthy volunteer test subjects (mean age=27.3 years, Standard Deviation (SD)=2.1; 5 women, 13 men) according to the ISEK standards [33] for collecting the sEMG data and the corresponding skeletal muscle force. All subjects provided informed consent as per clinical Institutional Review Board (IRB) protocol. Using a wet probe point muscle stimulator (RichMar Corporation, model number HV 1100) the motor points of the Flexor Digitorum Superficialis (FDS) were identified through the observed muscle action of the predominant movement of flexion of the first digit. The Flexor Digitorum Profundus (FDP) is also involved in the action of finger flexion, but it lies deeper than the FDS and hence the sEMG capturing includes both muscles in the finger motion. During a single episode of data collection, for each subject, the subject was asked to move only the index finger while fingers III-V were kept stationary and the wrist kept at neutral position. The primary sEMG sensor was placed on the motor point and the other two sensors placed adjacent to the motor point on the skin surface of test subject's dominant side at a distance of 1.5 cm on the either side of the sensor on the motor point.

Using a Delsys®, Bagnoli-16 channel EMG, DS-160, S/N-1116 system, the EMG data from the skin surface is captured. This acquisition system has an internal amplification gain of 1000 and a bandwidth of 20–450 Hz and line voltage isolation of 6000 VDC, 4200 VAC (RMS). Pronged DE 2.1 differential surface electrodes are placed perpendicular to the muscle fiber and a reference electrode which is placed on the subject's elbow are used to acquire the sEMG signals [34]. A model 402 single zone Force Sensitive Resistor (FSR) optimized for human touch control of electronic devices is used to acquire the skeletal muscle force. It has a 46.7 mm^2 active diameter area with a force sensitivity range of 0.1–100 N, force repeatability of $\pm 6\%$ and a continuous force resolution [35]. During the experiment each subject is made to perform a random grasping action (index finger flexion and extension) for 9–10 s with a moderate force production to avoid fatigue using a stress ball for added resistance. While doing so, the random grasping action finger force is applied on the FSR, which is mounted on the stress ball. Both the sEMG and the corresponding skeletal muscle force are synchronized and acquired

using NI LabVIEW™ with a single data acquisition board (DAQ NI 6024E) at a sampling rate of 2000 Hz. Since the content of the sEMG signal is in the range of 20–450 Hz, the sampling rate is chosen greater than twice of the Nyquist frequency.

3. Methodology

3.1. Filtering techniques

After acquiring the data from the sEMG sensors around an individual motor point, the sEMG data is rectified and filtered. For comparison between different filtration techniques, five different filters are used, i.e., two linear filters, (low-pass Chebyshev Type II filter and Butterworth filter), two non-linear filters (Bayesian Exponential filter and Bayesian Half-Gaussian filter) and Wavelet Transform (WT) based Daubechies (Db) 44. The low-pass Chebyshev type II filter is designed with a cutoff frequency of 550 Hz and a 12th order Butterworth filter is used. Since the Chebyshev Type II filter and the Butterworth filter are commonly used and easy to implement, the authors started with the basic filters and make a performance study [17]. The Bayesian filters employed in this work have the ability to record the rapid changes in the sEMG signal, rather than just smoothening it. Compared to the low-pass linear filters, these Bayesian filters will have a low error and high signal-to-noise ratio [18]. The latent driving signal x results in the EMG, which can be computed using an instantaneous conditional probability$P(\text{EMG}|x)$ [18]. This estimation algorithm uses the model of the conditional probability of the rectified EMG signal $emg = |\text{EMG}|$ [18]. As stated in [18], an exponential measurement model for the rectified EMG signal is given by

$$P(emg|x) = \exp\left(\frac{-emg}{x}\right)/x \tag{1}$$

Eq. (2) presents the Half-Gaussian measurement model for the rectified EMG signal [18]:

$$P(emg|x) = 2\exp\left(\frac{-emg^2}{2x^2}\right)/\sqrt{2\pi x^2} \tag{2}$$

The model for the conditional probability of the rectified EMG is a filtered random process with a random rate and the likelihood function for the rate evolves in time according to the Fokker–Planck partial equation [18]. The discrete time Fokker–Planck equation is given as

$$p(x,t-) \approx \alpha p(x-\varepsilon,t-1)+(1-2\alpha)p(x,t-1) + \alpha p(x+\varepsilon,t-1)+\beta+(1+\beta)p(x,t-1) \tag{3}$$

In Eq. (3), $\alpha$and $\beta$are two free parameters, where α is the expected rate of gradual amplitude drift and $\beta$is the expected rate of sudden shift in the signal, x is the latent driving signal, t is time index and ε is the discretization bin width of the latent driving signal x[18]. The filter parameters for the Half-Gaussian filter are selected in such a way that the effective EMG signal frequency content is no more than 500 Hz, according to the ISEK standards [33]. This latency requires employing huge buffer sizes which makes real-time implementation impossible. Hence, in this work we focused on algorithms that have the capacity to be implemented in real-time, using wavelets representing such an approach. A WT along with a Db 44 mother wavelet at 8 levels of decomposition is used in order to filter the sEMG data. One of our previous works included a comprehensive study of 324 mother wavelets for sEMG signals. The results indicated superior performance of the Db 44 wavelet method for processing biomedical related signals [36]. In this present work, the hypothesis stated in [36] "Db 44 wavelet method for processing biomedical related signals" is put to the test by processing the acquired sEMG signal using wavelets and utilizing the processed signal for modeling the underlying skeletal muscle force generated by individual fingers of the human hand. The single level of

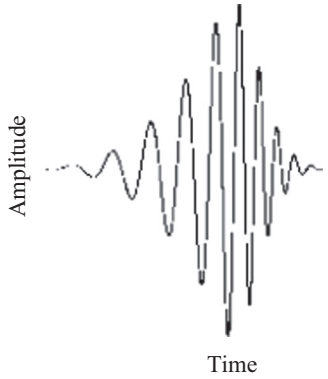

Fig. 3. Daubechies 44 (Db 44) mother wavelet structure

Discrete Wavelet Transform (DWT) is given as

$$u_{fi}[n] = (u_{ufi}g_i)[n] = \sum_{k=-\infty}^{\infty} u_{ufi}[k]g_i[n-k], \tag{4}$$

$$u_{fi_{low}}[n] = \sum_{k=-\infty}^{\infty} u_{ufi}[k]g_i[2n-k] \tag{5}$$

$$u_{fi_{high}}[n] = \sum_{k=-\infty}^{\infty} u_{ufi}[k]h_i[2n-k] \tag{6}$$

where i is the corresponding sensor, u_{ufi} is the unfiltered sEMG signal, u_{fi} — Filtered sEMG signal, g_i — Co-efficient of the low-pass filter, h_i — Co-efficient of the high pass filter. g_i and h_i are chosen based on the ISEK standards to eliminate any noise in the sEMG signal.

Fig. 3 shows the Db 44 structure; the structural similarity of the mother wavelet and the sEMG signal makes it more desirable to employ the order of 44 for the Db filter in this work.

Fig. 4 shows the WT based Db 44 sEMG filtered data, and the x-axis shows the sEMG data points for 9 s duration. Fig. 4a shows the unfiltered and filtered (using the Db 44 wavelet) sEMG signals. Fig. 4b shows the decomposition coefficients of the sEMG signal at each level and Fig. 4c depicts the reconstructed approximation of the sEMG signal based on the decomposition coefficients at each level.

3.2. sEMG/skeletal muscle force modeling

After pre-processing the data, sEMG data $u_1(t)$, $u_2(t)$ and $u_3(t)$ from the three sensors and their corresponding skeletal force signal $Y(t)$ are used to identify the dynamic relationship between them by utilizing the SI technique. Three SI models – linear Output Error (OE) models, nonlinear Wiener-Hammerstein (WH) models and frequency domain Spectral Analysis Frequency Dependent Resolution (SPAFDR) models – are investigated to model the dynamics, the frequency content of the sEMG signal and the corresponding skeletal muscle force.

3.3. Linear and nonlinear models

The modeling of linear and nonlinear dynamics of the sEMG signal and the corresponding skeletal muscle force is achieved by using the WH model structure which is shown in Fig. 5.

The mathematical representation of the modeling is given by,

$$w(t) = f(u(t)), \tag{7}$$

$$x(t) = \frac{B(q)}{F(q)}w(t-n_k)+e(t), \tag{8}$$

$$y(t) = h(x(t)), \tag{9}$$

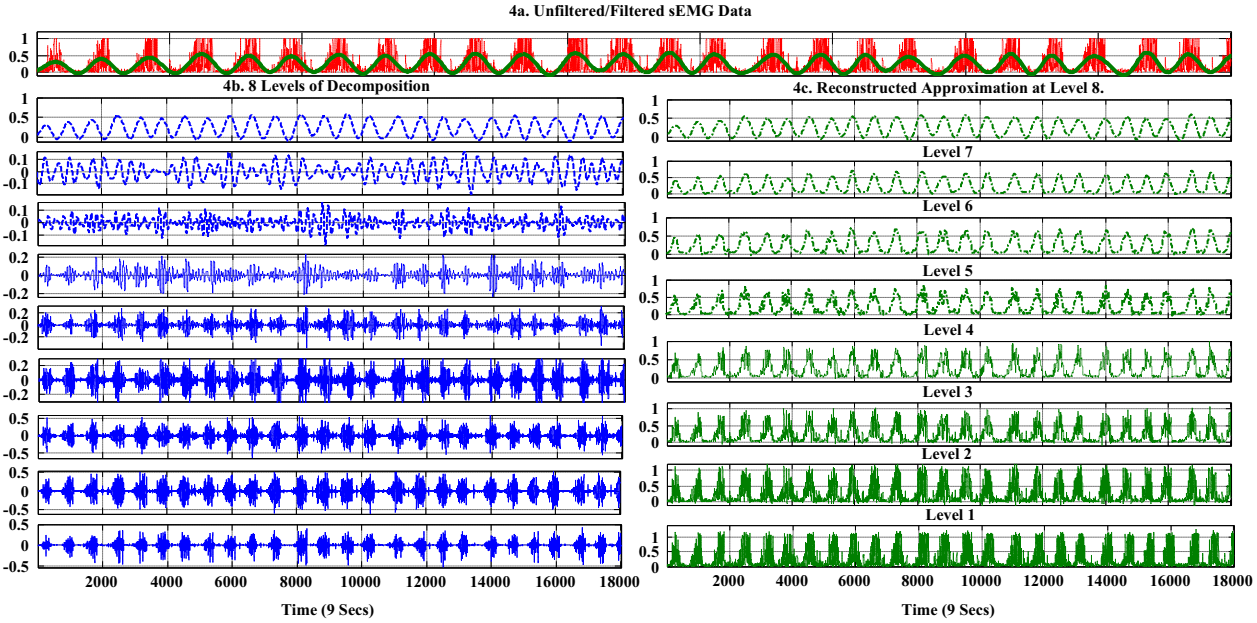

Fig. 4. Shows the wavelets based sEMG filtered data, and the x-axis shows the sEMG data points for 9 s duration. (4a) Filtered and unfiltered sEMG signal using wavelets Daubechies 44 filter. (4b) 8 levels of decomposition co-efficient for the sEMG signal using wavelet Daubechies 44 filter, (4c) Reconstructed approximation of sEMG signal at each level using wavelet Daubechies 44 filter.

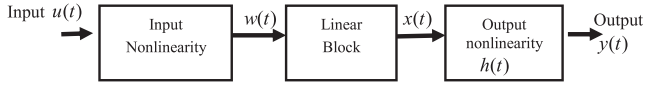

Fig. 5. Wiener Hammerstein (WH) model structure with input and output non-linearity classes of the input and the output signals respectively and the linear classes.

where $u(t)$ is the preprocessed sEMG signal and $y(t)$ is the skeletal muscle force signal, f and h are nonlinear functions/classes, $w(t)$ and $x(t)$ are internal variables, $B(q)$ and $F(q)$ are polynomials, q is the back shift operator, and $e(t)$ is the output error residual between measured quantity and estimated quantity. From (8), the WH model structure utilizes a linear OE model, which is given by,

$$y(t) = \frac{B(q)}{F(q)}u(t-n_k) + e(t) \tag{10}$$

where n_k is the system delay and t is time index. Since linear OE model is a part of the WH structure from (8) and (10), WH captures both the linear and non-linear dynamics of the sEMG and the corresponding skeletal muscle force signal.

From (7) and (9), the WH captures the non-linear dynamics, so a performance comparison of various standard nonlinear classes is made. Table 1 shows the mean percentage Pearson Correlation coefficient for different non linearity classes for 18 subjects. The 8th order 1-dimensional polynomial class yields better performance in approximating the non-linear dynamics between the sEMG and skeletal muscle force signals than to the other nonlinear classes with higher correlation and the lower Standard Deviation. Hence, the authors continued to utilize the 1-dimensional polynomial class for all the WH models to perform the study further. M_2 is the WH model identified from the sensor data $u_2(t)$ located on the motor unit. This model provides a better correlation between the sEMG and the skeletal muscle force data when compared to the models M_1 and M_3 identified from the sensor data $u_1(t)$ and $u_3(t)$ respectively.

3.4. Spectral models

The frequency content of the sEMG signal is captured and modeled using the SPAFDR spectral modeling technique. From the past research, it is evident that the SPAFDR models are best suited for modeling the frequency content of the sEMG data, [37]. The SPAFDR modeling algorithm is given as follows:

Consider a linear dynamic system,

$$y(t) = G(q)u(t) + v(t), \tag{11}$$

where $G(q)$ is the transfer function providing the dynamic relationship between sEMG and force. $G(q)$ is evaluated on the unit circle $G(q = e^{j\omega})$, where ω is a frequency value and is chosen according to the ISEK standards. For the linear dynamic system (11) the SPAFDR frequency response function returns a transfer function estimate $G(e^{j\omega})$ as well as the spectrum additive noise. The sEMG and the skeletal muscle force data are converted into frequency domains $U(\omega)$ and $Y(\omega)$. The frequency domain data are formed as convolution as follows:

$$\text{avg}\left[\frac{Y(\omega)\text{conj}U(\omega) \times U(\omega)\text{conj}Y(\omega)}{\omega}\right], \tag{12}$$

with a desired resolution of $\zeta(k) = 2(w(k+1) - w(k)$, w is the row vector of the frequencies ω, k is the frequency resolution. The frequency-response function $\hat{G}_N(e^{j\omega})$ and the output noise spectrum $\hat{\Phi}_v(\omega)$ are computed as

$$\hat{G}_N(e^{i\omega}) = \frac{\hat{\Phi}_{yu}(\omega)}{\hat{\Phi}_u(\omega)}, \tag{13}$$

$$\Phi_v(\omega) = \lambda T |H(e^{j\omega T})|^2. \tag{14}$$

where $\hat{\Phi}_{yu}(\omega)$ and $\hat{\Phi}_u(\omega)$ are the additive and input noise spectrum respectively, $H(e^{j\omega T})$ is the polynomial coefficients, λ is the estimated

Table 1
Mean percentage correlation co-efficient for non linearity class.

Nonlinearity classes	M_1	M_2	M_3
Piecewise linear	25.0 ± 4.5	32.7 ± 4.0	30.9 ± 4.3
Sigmoid	20.5 ± 5.6	27.3 ± 5.3	25.8 ± 5.4
Dead zone	15.3 ± 4.8	22.4 ± 4.2	19.5 ± 4.7
Saturation	35.0 ± 4.9	38.2 ± 4.6	36.0 ± 5.3
Unit gain	51.3 ± 4.7	55.9 ± 4.4	53.6 ± 5.0
1D-polynomial	70.05 ± 3.6	72.67 ± 3.5	62.23 ± 3.9

variance and T is the sampling time. The frequency response model can be realized using an OE model structure (10).

4. Fusion algorithms

In this paper, two different fusion algorithms are proposed. They are used for fusing time domain non-linear models and frequency domain spectral models.

4.1. Probability analysis based fusion algorithm (PAFA)

After modeling the dynamics relating sEMG and finger force data, non-linear and spectral models are fused individually using PAFA. PAFA utilizes three different model selection criteria i.e., the Akaike Information Criterion (AIC), the Kullback Information Criterion (KIC) and the Bayesian Information Criterion (BIC). The AIC criterion is an asymptotically unbiased estimator of the Kullback's directed divergence between the true model and the estimated model. The dissimarility between the two statistical models is called relative entropy or I-divergence. When the dimension of the candidate model increases compared to the sample size, then the AIC becomes a negatively unbiased estimator. A biased version of AIC was proposed in [38] to overcome this. The corrected form of Akaike's asymptotic bias is given by

$$\mathrm{AIC} = -2\ln R_i + 2p_i \tag{15}$$

Hurvich [28] gave the biased corrected version as

$$\mathrm{AIC}(p_i) = \frac{n}{2}\log R_i + \frac{(p_i+1)n}{n-p_i-2} \tag{16}$$

where 'n' is the number of data points, R_i is the residual square norm and p_i is the order of the ith model (M_i).

KIC is an asymmetric measure of the models' dissimilarity, obtained by the sum of two directed divergences, known as Kullback's symmetric or J-divergence [38],

$$\mathrm{KIC}(p_i) = \frac{n}{2}\log R_i + \frac{(P_i+1)n}{n-p_i-2} - n\psi\left(\frac{n-p_i}{2}\right) + g(n) \tag{17}$$

where$g(n) = n \times \log(n/2)$, ψ — digamma function.

The Bayesian Information Criterion (BIC) was introduced by Schwarz in 1978, [39]. It can be calculated by approximating the evidence ratios of models, which is known as the Bayes factor [39]. Bayesian inference is the quantity that updates the probability of the prior model to the posterior model probability as given by the following equation:

$$\mathrm{BIC}(p_i) = \frac{n}{2}\log R_i + \frac{p_i+1}{2}\log n \tag{18}$$

Multiple model fusion technique as explained in [40–42] is based on assigning a particular probability to each individual model. Each model is extracted by using SI from the recorded finger force and sEMG data. The following five steps give the generalized fusion algorithm for $k$number of sensors. In this work, we used three sEMG sensors.

Step 1: Considering the sEMG data $u(t)$as input and force data $Y(t)$ as output identify the sEMG/force Models $M_1(t), M_2(t), ..., M_k(t)$.

Step 2: Calculate the residual square norm i.e., $R_i = Y - \Phi_i\hat{\theta}_i = ||Y-\hat{Y}||$, Where $\hat{\theta}_i = \{\Phi_i{}^T\Phi_i\}^{-1}\Phi_i^T Y$, and

$$\Phi = \begin{bmatrix} Y^T & u_{p-1}^T & Y_{p-1}^T & u_1^T \\ Y_{p+1}^T & u_{p+1}^T & Y_p^T & u_2^T \\ \cdots & \cdots & \cdots & \cdots \\ Y_{n-1}^T & u_{n-1}^T & Y_{n-2}^T & u_{n-p}^T \end{bmatrix}$$

Step 3: After obtaining the residual square norm, compute the model criteria coefficients using (16-18).

Step 4: The model probability can be computed using,

$$p(M_i(t)|Z) = \frac{e^{-l_i}}{\sum_{j=1}^{k} e^{-l_j}}$$

where Z is the filtered sEMG data and Iis the number of sensors.

Step 5: The fused model output can be calculated using,

$$\hat{Y}_f = \sum_{i=1}^{k} p(M_i(t)|Z)\hat{Y}_i.$$

4.2. Optimized linear model fusion algorithm (OLMFA)

The Optimized Linear Model Fusion Algorithm (OLMFA) utilizes a simple elitism based GA. OLMFA is computed as follows:

For the linear model structure given in (9), the continuous time representation of the OE model structure is given by,

$$G(z) = \frac{B(z)}{F(z)} = \frac{b_{nb}z^{(nb-1)}b_{nb-1}z^{(nb-2)} + \ldots + b_1}{z^{nf} + f_{nf}z^{nf-1} + \ldots + f_1} \tag{19}$$

Similar to the discrete-time case, the orders of the numerator and denominator are determined by nb and nf. For multi-input systems, nb and $nf$are row vectors. b,f are the coefficients of the numerator and denominator polynomials respectively.

Based on the poles of the three linear models, corresponding to each sensor, a Multiple Input Single Output (MISO) transfer function $H$is constructed. While the denominators of the respective individual transfer functions (corresponding to each OE model) are superimposed on the new MISO transfer function, the corresponding zeros are found through the use of a GA. Generally GAs can find global optimum points if an elitism scheme is used and a sufficient number of generations are allowed in the algorithm [43]. This optimization algorithm is rather computationally expensive, but since there was no computational time requirement, one is free to use GA rather than other intelligence based algorithms. Chromosomes are constructed by designating each zero of a numerator as a gene. Since a discrete time model is utilized, the search area is limited to the unit circle and the resulting MISO model is decreased to be minimum phase. The number of potential zeros was set to the order of the corresponding denominator.

The following fusion technique is applied to the sEMG-force identification model:

Step 1: Considering the sEMG data $u(t)$ as input force data and Y as output identify the sEMG/force linear and spectral Models $M_1(s)$, $M_2(s), ..., M_k(s)$.

Step 2: Using GA, a hybrid transfer function $H(s)$ is computed as: $C = [p_1, p_2, ...p_N]$, where $p_1, p_{2,...,}p_N$, are the chromosomes.

Step 3: Initial population is computed by: $IP = (H-L)*R_N + L$,

where H is the highest number in the parameter range, L is the lowest number in the parameter range, R_N is the random $\{N_{IP}-N_{PA}\}$, N_{IP} is the population size of generations and N_{PA} is the number of sensors.

Step 4: Mating: $\alpha_{GA} = \mathrm{roundup}\{N_{PA}\}$, $A_1 = [a_{m_1}, a_{m_2}, \ldots a_{m_\alpha}, \ldots a_{m_N}]$, $A_2 = [a_{d_1}, a_{d_2}, \ldots a_{d_\alpha}, \ldots a_{d_N}]$. where a_{m_N} is the n^{th} parameter in the mother chromosome and a_{d_N} is the nth parameter in the father chromosome

Then

$$A_{new1} = a_{m_\alpha} - \beta_{GA}[a_{m_\alpha} - a_{d_\alpha}], A_{new2} = a_{d_\alpha} + \beta_{GA}[a_{m_\alpha} - a_{d_\alpha}]$$

where β_{GA} is the random number on the interval [0,1].

Then

$$os_1 = [a_{m_1}, a_{m_2}, \ldots a_{new_1}, \ldots a_{d_N}], os_2 = [a_{d_1}, a_{d_2}, \ldots a_{new_2}, \ldots a_{m_N}],$$

where os_1, os_2 are the off springs.

Step5: Mutation: $M_R \times T_{NP} = N_{PM}$ where M_R is the mutation rate, T_{NP} is the total number of parameters and N_{PM} is the number of parameters to be mutated.

Step 6: Compute the cost of each chromosome using

$$J = \lambda \sum_{i=1}^{n} |y(t-i) - \hat{y}_f(t-i)|^2 + \nu(corr[y, \hat{y}_f])$$

where λ and ν are weighting coefficients and *'corr'* is the correlation function.

Step 7: The Fitness function F_f is computed by,

$$F_f = \int_{t_0}^{t_f} (\hat{Y}(t) - Y(t))^2 dt = \int_{t_0}^{t_f} \phi^2(t) dt.$$

where t_0 and t_f are the initial and final time values, $\hat{Y}(t)$ is the fusion model estimated force and $Y(t)$ is the actual force from the FSR.

Step 8: The objective function is set as the error square of the resulting MISO system. $H(s)$ (see Appendix) is given as

$$H(z) = \begin{pmatrix} \frac{A_{1,1}z^n + A_{1,2}z^{n-1} + \ldots + A_{1,n+1}}{B_{1,1}z^n + B_{1,2}z^{n-1} + \ldots + B_{1,n+1}} \\ \frac{A_{2,1}z^n + A_{2,2}z^{n-1} + \ldots + A_{2,n+1}}{B_{2,1}z^n + B_{2,2}z^{n-1} + \ldots + B_{2,n+1}} \\ \frac{A_{3,1}z^n + A_{3,2}z^{n-1} + \ldots + A_{3,n+1}}{B_{3,1}z^n + B_{3,2}z^{n-1} + \ldots + B_{3,n+1}} \end{pmatrix}$$

where A's and B's are the numerator and the denominator coefficients respectively of individual transfer function and$n$ is the order of the system.

Step 9: Feed new data sets to the Multiple Input Single Output (MISO) transfer function $H(z)$ will result in an estimated fusion based force $\hat{Y}(t)$.

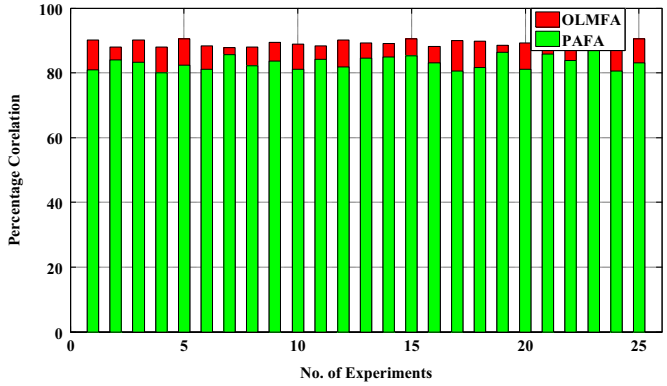

Fig. 6. Comparison of OLMFA and PAFA for 25 different test data from the 18 subjects. X–axis represents the validation experiments with the k-fold cross validation data and Y-axis represents the percentage correlation between the actual force from the FSR and the fusion algorithm estimated force.

4.3. Comparison of PAFA and OLMF

Since PAFA is based on probability analysis, it is capable of fusing the non-linear models, whereas the OLMFA cannot fuse non-linear models. Application of GA enables OLMFA to overcome the local minima [45]. Some additional advantages of it are that it can handle a large number of parameters that can be handled easily such that they do not require the traditional approach of taking derivatives, it results in a set of optimum candidate solutions rather than a single candidate solution, and it works well with experimental data as well as simulated data.

From step 7 of the OLMFA, the error square of the measured and estimated forces is formulated as a fitness function. Hence OLMFA can be used for the fusion of linear models for any application demanding performance accuracy where performance time is not restricted. However, applying this approach to non-linear model structures would require linearization and approximations to optimize them. PAFA can be employed for both linear and non-linear models without approximations where performance time is restricted. Since SPAFDR models are realized using linear OE models, Fig. 6 gives the percentage correlation coefficients comparison between OLMFA and PAFA for the SPAFDR models for 25 different test data from the 18 subjects' sEMG and the corresponding skeletal muscle force data. It is evident from Fig. 6 that OLMFA performs slightly better than PAFA in terms of percentage correlation coefficients between actual force ($Y(t)$) and fusion estimated force ($\hat{Y}(t)$).

5. Results and discussion

Table 2 shows the mean Pearson correlation coefficients and the mean relative error and their standard deviation (σ) for the non-linear WH models and the SPAFDR spectral models constructed from the sEMG data using three sensors and the corresponding skeletal muscle force for 18 test subjects. M_2 is the model constructed from the sensor data u_2(t) located on the motor unit and provides a better correlation between the sEMG and the skeletal muscle force data when compared with M_1 and M_3 constructed from sensor data u_1(t) and u_3(t), respectively Table 2 also provides the comparison of the mean correlation and the standard deviation between the actual force and individual WH and SPAFDR model estimated forces for the five different filters. Fifty four different WH and SPAFDR models are constructed for the sEMG/skeletal muscle force data from the three sEMG sensors of the 18 test subjects. The mean of the 54 (18 subjects and 3 sensors) percentage Pearson correlation coefficient's and the relative error for five different filters using the two modeling techniques is presented in Table 2. It is evident from Table 2 that the WT Db 44 demonstrates better performance when compared with the other

Table 2
Mean and standard deviation of percentage pearson correlation coefficients and relative error comparision of five different filters for WH and SPAFDR Models For 18 test subjects

SI technique	Models	BW		CS		EXP		HG		WT Db 44	
		$\mu_\rho \pm \sigma_\rho$	$\mu_\eta \pm \sigma_\eta$	$\mu_\rho \pm \sigma_\rho$	$\mu_\eta \pm \sigma_\eta$	$\mu_\rho \pm \sigma_\rho$	$\mu_\eta \pm \sigma_\eta$	$\mu_\rho \pm \sigma_\rho$	$\mu_\eta \pm \sigma_\eta$	$\mu_\rho \pm \sigma_\rho$	$\mu_\eta \pm \sigma_\eta$
Nonlinear WH models	M_1	52.9 ± 3.6	45.2 ± 3.2	61.1 ± 3.8	43.3 ± 3.1	55.2 ± 3.7	45.7 ± 3.4	**58.7 ± 2.7**	**36.3 ± 2.9**	**70.0 ± 1.9**	**37.6 ± 1.8**
	M_2	*54.3 ± 3.5*	*43.6 ± 3.1*	*62.5 ± 3.6*	*42.6 ± 3.0*	*56.2 ± 3.6*	*44.9 ± 3.1*	**67.7 ± 2.5**	**35.5 ± 2.8**	**72.6 ± 1.7**	**32.4 ± 1.6**
	M_3	51.2 ± 3.6	47.3 ± 3.8	58.6 ± 3.7	44.0 ± 3.2	50.7 ± 3.7	46.8 ± 3.3	**57.5 ± 2.6**	**38.0 ± 2.9**	**62.2 ± 1.8**	**39.9 ± 1.7**
Spectral SPFRD models	M_1	49.8 ± 3.9	48.5 ± 3.9	55.3 ± 3.8	48.5 ± 3.2	50.0 ± 3.9	48.7 ± 3.4	**57.6 ± 2.6**	**39.8 ± 2.8**	**61.8 ± 1.9**	**38.2 ± 1.8**
	M_2	*57.6 ± 3.6*	*45.7 ± 3.0*	*58.5 ± 3.7*	*43.4 ± 3.1*	*52.5 ± 3.7*	*46.2 ± 3.2*	**69.7 ± 2.6**	**36.4 ± 2.8**	***70.4* ± *1.5***	***33.0* ± *1.7***
	M_3	53.4 ± 3.7	46.9 ± 3.2	56.2 ± 3.7	46.2 ± 3.1	51.9 ± 3.8	47.0 ± 3.4	**65.6 ± 2.7**	**38.7 ± 2.9**	**68.2 ± 1.7**	**35.2 ± 1.8**

μ_ρ—mean percentage correlation, σ_ρ—correlation standard deviation, μ_η—mean percentage relative error, σ_η—relative error standard deviation, BW— Butterworth filter, CS—Chebyshev Type-II filter, EXP—Bayesian Exponential filter, HG—Bayesian Half-Gaussian filter, WT—Wavelet Transforms.

four filters for both time domain non-linear WH modeling and frequency domain modeling in terms of mean Pearson correlation coefficients and relative errors with the lowest standard deviation. From Table 2 it can also be inferred that HG filter gives the second best performance when compared to the other three filters. The mathematical construction of the HG filter requires employing a window to compute the probability, which makes it unrealistic to implement it in real-time because of the large buffer size. Hence the authors choose to utilize the WT Db 44 to continue with further analysis.

The wavelet filtered data from the 18 subjects is fed into the fusion algorithms. Fig. 7 shows the actual force ($Y(t)$) and the fusion algorithm estimated force ($\hat{Y}_f$) plotted together using PAFA for WH models. From Fig. 7 we can infer that PAFA estimated force ($\hat{Y}_f$) tracks the changes in the actual force and matches it to the actual force ($Y(t)$). Fig. 8 shows the actual force ($Y(t)$) and the fusion algorithm estimated force ($\hat{Y}_f$) plotted together using PAFA for SPAFDR models. Fig. 9 shows the plot between actual force from FSR ($Y(t)$) and the OLMFA estimated force ($\hat{Y}(t)$) SPAFDR models. From Figs. 8 and 9 it is evident that OLMFA is performing better than PAFA for the SPAFDR models for the above mentioned reasons.

Tables 3 and 4 show the fusion algorithm comparison for WH and the SPAFDR models respectively. From these two tables it can be seen that the sensor data fusion improves the percentage correlation (ρ) and reduces the percentage relative error (η) between the actual force ($Y(t)$) and the fusion algorithm estimated force ($\hat{Y}_f$) when compared to individual model force estimates. It is clear from Table 3 that the KIC based PAFA works best for both WH and SPAFDR models indicating a high correlation between the fusion algorithm estimated force ($\hat{Y}_f$) and the actual force ($Y(t)$), and also indicating low standard deviation (σ) for percentage correlation and the percentage relative error (η). It is also clear from Table 4 that OLMFA yields higher percentage correlation and low percentage relative error for SPAFDR

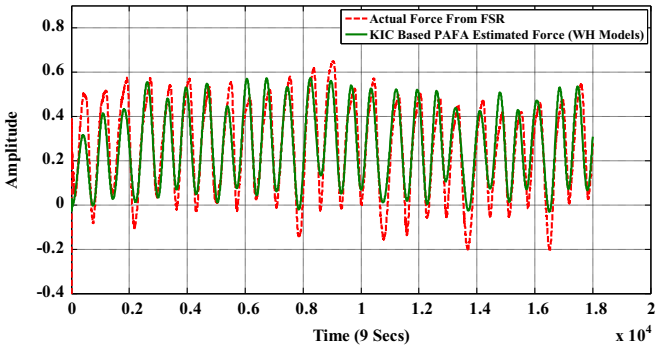

Fig. 7. PAFA estimated force and the actual force plotted together for WH models during a random grasping action and the X-axis represents the number of data points collected for a duration of 9 s.

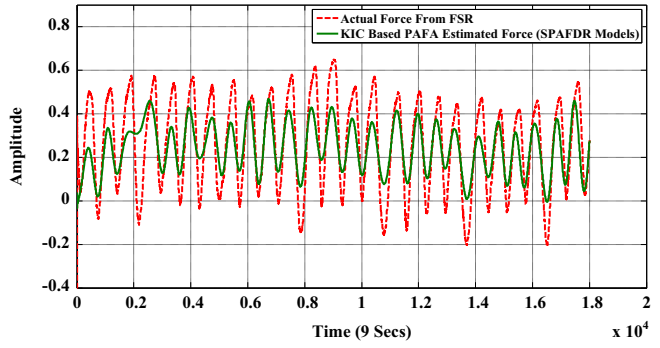

Fig. 8. PAFA estimated force and the actual force plotted together for SPAFDR Models during a random grasping action and the x-axis represents the number of data points collected for a duration of 9 s.

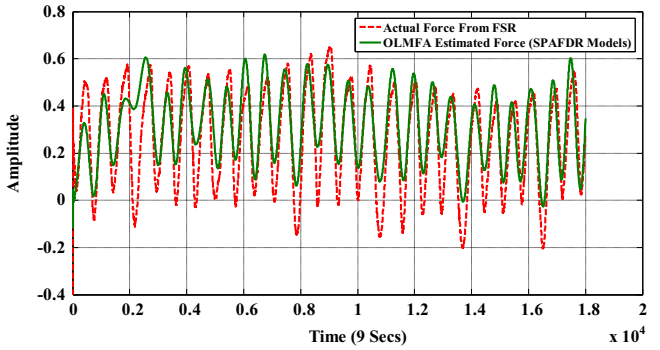

Fig. 9. OLMFA estimated force and the actual force from the FSR plotted together for SPAFDR Models during a random grasping action and the X-axis represents the number of data points collected for a duration of 9 s.

models. Table 4 also indicates a low standard deviation for both the percentage correlation and the relative error. Tables 3 and 4 also show that the fusion based estimated force provides better corelation than the individual SI based WH and SPAFDR models.

To test the variability of the results, cross validation is done and Tables 3 and 4 provide the mean and standard deviation of the percentage correlation (ρ) and the relative error (η) for k-fold cross validation data from 18 subjects. Using the k-fold cross validation, data from each sensor is divided into 18 different subsets. Each individual model M_1, M_2 and M_3 and the fusion based estimates are validated with the k-fold cross validation subset data from the 18 subjects. Therefore the mean and standard deviation of the percentage correlation and the relative error for each individual model and the fusion estimates for 18 k-fold validation subset data are presented in Tables 3 and 4. It can be inferred from Tables 3 and 4 that M_2 is performing better when compared withM_1 and $M_3$for the cross validation data. It is also observed that the standard deviation for the percentage relative error and the percentage correlation is also low for M_2 when compared with the other models M_1 and M_3 for both WH and SPAFDR models. Therefore, it can be inferred that the sensor located directly on the motor point is giving data that is more suitable to extract useful information when compared with the other sensory data. In the WH models, M_1 is yielding the next best performance when compared with M_3 except for subjects 4, 8, 10 and 15. Also, for the SPAFDR models, M_3 is yielding a better performance than M_1 except for subjects 2, 5, 12, 16 and 18. This could be due to motor point location in reference to sensor alignment and crosstalk and noise interference. Therefore, it is clear that the WH and the SPAFDR capture different EMG content. It can also be inferred from Tables 3 and 4 that KIC is performing better when compared to AIC and BIC for both the WH and SPAFDR models. Since KIC is an asymmetric measure of the models dissimilarity it would work better for the bio-medical signals when compared to AIC and BIC.

Fig. 10 gives the frequency response in comparison to the OE, WH and SPAFDR sEMG/Skeletal muscle force models. It is interesting to note that all the three different model types capture different bands of frequencies. This indicates that OE, WH and SPAFDR models are capturing additional and different information. This difference can be due to a number of reasons, such as model order selection, input design [44,45] for the experiment and also the model structure.

Thus we fused the entire time domain linear and non-linear WH and frequency domain SPAFDR models using KIC based PAFA. Fig. 11 shows the actual experimental force and the overall hybrid fusion algorithm estimated force plotted together. The overall fusion algorithm estimated force yields a 96% mean correlation and a 3.9% mean relative error with a standard deviation of ± 1.3 and ± 0.9 respectively between the overall hybrid fusion algorithm estimated and the actual force for 18 test subjects' k-fold cross validation data.

It is also clear from Fig. 11 that both the WH and SPAFDR models are capturing the non-linear dynamics and frequency content of the

Table 3
Fusion algorithm comparison of mean and standard deviation of correlation coeffciants and relative error for 12,000 data points for WH models using WT using k-fold validation data from 18 subjects. The last row represents the overall mean for all the 18 subjects

Subjects	Individual models						Fusion							
	M_1		M_2		M_3		AIC		BIC		KIC		OLMFA	
	$\mu_\rho \pm \sigma_\rho$	$\mu_\eta \pm \sigma_\eta$	$\mu_\rho \pm \sigma_\rho$	$\mu_\eta \pm \sigma_\eta$	$\mu_\rho \pm \sigma_\rho$	$\mu_\eta \pm \sigma_\eta$	$\mu_\rho \pm \sigma_\rho$	$\mu_\eta \pm \sigma_\eta$	$\mu_\rho \pm \sigma_\rho$	$\mu_\eta \pm \sigma_\eta$	$\mu_\rho \pm \sigma_\rho$	$\mu_\eta \pm \sigma_\eta$	$\mu_\rho \pm \sigma_\rho$	$\mu_\eta \pm \sigma_\eta$
1	71.0 ± 1.9	38.3 ± 1.9	72.5 ± 1.8	31.2 ± 1.8	63.2 ± 1.9	39.4 ± 1.9	81.6 ± 1.7	25.4 ± 1.7	76.1 ± 1.8	30.2 ± 1.8	**92.3 ± 1.5**	**17.7 ± 1.5**	NA	NA
2	68.1 ± 1.9	36.9 ± 1.9	72.2 ± 1.8	32.5 ± 1.9	65.9 ± 1.8	37.5 ± 1.9	82.1 ± 1.7	26.8 ± 1.7	76.2 ± 1.8	31.6 ± 1.8	**93.3 ± 1.6**	**17.0 ± 1.6**	NA	NA
3	70.9 ± 1.8	37.4 ± 1.9	73.0 ± 1.8	32.7 ± 1.9	67.5 ± 1.8	37.8 ± 1.9	81.4 ± 1.7	25.5 ± 1.7	75.4 ± 1.8	31.8 ± 1.8	**92.9 ± 1.4**	**16.7 ± 1.5**	NA	NA
4	65.2 ± 1.9	38.0 ± 1.9	72.8 ± 1.9	31.3 ± 1.8	69.5 ± 1.9	36.2 ± 1.9	82.2 ± 1.8	25.9 ± 1.7	72.6 ± 1.8	29.7 ± 1.8	**92.7 ± 1.5**	**18.8 ± 1.5**	NA	NA
5	71.7 ± 1.9	35.3 ± 1.8	74.5 ± 1.8	33.8 ± 1.8	62.2 ± 1.9	37.5 ± 1.9	81.0 ± 1.7	27.4 ± 1.7	73.4 ± 1.8	28.9 ± 1.8	**92.5 ± 1.5**	**17.0 ± 1.6**	NA	NA
6	70.0 ± 1.8	34.0 ± 1.9	73.6 ± 1.8	32.3 ± 1.8	64.2 ± 1.9	36.7 ± 1.9	83.6 ± 1.7	26.0 ± 1.6	72.7 ± 1.8	30.6 ± 1.8	**92.9 ± 1.5**	**17.7 ± 1.5**	NA	NA
7	68.6 ± 1.9	37.6 ± 1.9	71.6 ± 1.8	34.0 ± 1.9	65.6 ± 1.8	39.7 ± 1.9	78.9 ± 1.8	27.6 ± 1.7	72.5 ± 1.8	31.5 ± 1.8	**93.1 ± 1.6**	**18.8 ± 1.5**	NA	NA
8	69.1 ± 1.9	39.7 ± 1.8	73.2 ± 1.9	33.0 ± 1.8	70.0 ± 1.9	37.8 ± 1.9	82.6 ± 1.7	25.6 ± 1.7	75.2 ± 1.8	32.6 ± 1.7	**92.3 ± 1.5**	**16.4 ± 1.5**	NA	NA
9	68.9 ± 1.9	35.7 ± 1.9	71.4 ± 1.8	32.5 ± 1.8	64.3 ± 1.9	36.8 ± 1.9	81.6 ± 1.7	25.8 ± 1.7	73.9 ± 1.8	31.0 ± 1.8	**92.7 ± 1.5**	**18.3 ± 1.6**	NA	NA
10	67.3 ± 1.8	37.7 ± 1.8	73.8 ± 1.7	35.2 ± 1.7	69.4 ± 1.8	36.3 ± 1.8	82.9 ± 1.6	27.6 ± 1.7	75.6 ± 1.7	33.7 ± 1.7	**93.8 ± 1.4**	**17.4 ± 1.5**	NA	NA
11	70.2 ± 1.9	36.6 ± 1.9	73.3 ± 1.7	35.9 ± 1.8	64.1 ± 1.8	38.9 ± 1.9	82.4 ± 1.7	26.8 ± 1.7	74.6 ± 1.8	32.1 ± 1.8	**92.0 ± 1.6**	**17.3 ± 1.6**	NA	NA
12	70.0 ± 1.8	38.2 ± 1.9	74.5 ± 1.8	37.2 ± 1.8	62.5 ± 1.8	39.9 ± 1.8	82.4 ± 1.7	28.4 ± 1.8	75.0 ± 1.8	31.6 ± 1.8	**91.6 ± 1.5**	**18.7 ± 1.5**	NA	NA
13	69.7 ± 1.9	37.5 ± 1.9	72.3 ± 1.8	35.2 ± 1.8	63.9 ± 1.9	38.0 ± 1.9	83.0 ± 1.7	27.2 ± 1.7	73.8 ± 1.7	32.0 ± 1.8	**93.5 ± 1.5**	**17.5 ± 1.5**	NA	NA
14	71.2 ± 1.9	36.8 ± 1.9	72.6 ± 1.8	33.7 ± 1.8	62.3 ± 1.9	38.4 ± 1.8	81.2 ± 1.7	29.0 ± 1.7	74.6 ± 1.8	33.4 ± 1.7	**92.5 ± 1.5**	**17.8 ± 1.5**	NA	NA
15	64.9 ± 1.9	37.7 ± 1.9	72.2 ± 1.8	34.4 ± 1.8	67.5 ± 1.8	35.3 ± 1.9	82.7 ± 1.7	28.7 ± 1.7	73.3 ± 1.8	32.0 ± 1.8	**92.7 ± 1.6**	**18.9 ± 1.5**	NA	NA
16	71.6 ± 1.8	36.6 ± 1.8	73.9 ± 1.7	33.6 ± 1.8	61.9 ± 1.8	38.6 ± 1.8	82.5 ± 1.6	27.2 ± 1.7	76.6 ± 1.7	31.9 ± 1.8	**92.8 ± 1.5**	**16.2 ± 1.5**	NA	NA
17	70.1 ± 1.9	37.6 ± 1.9	73.7 ± 1.8	32.2 ± 1.8	63.0 ± 1.9	38.4 ± 1.9	81.2 ± 1.7	26.9 ± 1.7	74.2 ± 1.8	32.3 ± 1.8	**92.7 ± 1.5**	**17.3 ± 1.5**	NA	NA
18	68.9 ± 1.8	36.0 ± 1.9	72.3 ± 1.8	34.6 ± 1.8	64.6 ± 1.9	37.8 ± 1.9	82.0 ± 1.7	27.3 ± 1.7	74.3 ± 1.7	32.6 ± 1.8	**93.0 ± 1.6**	**17.7 ± 1.5**	NA	NA
	69.3 ± 1.8	37.0 ± 1.8	72.9 ± 1.8	33.6 ± 1.8	65.0 ± 1.8	37.8 ± 1.8	81.9 ± 1.7	26.9 ± 1.7	74.4 ± 1.8	31.6 ± 1.8	92.7 ± 1.5	17.6 ± 1.5	NA	NA

NA — Not applicable

Table 4
Fusion algorithm comparison of mean and standard deviation of coeraltion coeffciants and relative error for SPAFDR models for 12,000 data points using WT using k-fold validation data from 18 subjects. The last row represents the over all mean for all the 18 subjects.

Subjects	Individual SPAFDR model						SPAFDR models data fusion							
	M_1		M_2		M_3		AIC		BIC		KIC		OLMFA	
	$\mu_\rho \pm \sigma_\rho$	$\mu_\eta \pm \sigma_\eta$	$\mu_\rho \pm \sigma_\rho$	$\mu_\eta \pm \sigma_\eta$	$\mu_\rho \pm \sigma_\rho$	$\mu_\eta \pm \sigma_\eta$	$\mu_\rho \pm \sigma_\rho$	$\mu_\eta \pm \sigma_\eta$	$\mu_\rho \pm \sigma_\rho$	$\mu_\eta \pm \sigma_\eta$	$\mu_\rho \pm \sigma_\rho$	$\mu_\eta \pm \sigma_\eta$	$\mu_\rho \pm \sigma_\rho$	$\mu_\eta \pm \sigma_\eta$
1	62.7 ± 1.9	40.7 ± 1.9	71.7 ± 1.8	33.6 ± 1.8	67.1 ± 1.9	39.9 ± 1.9	78.5 ± 1.7	29.5 ± 1.7	73.6 ± 1.8	32.1 ± 1.8	**86.0 ± 1.6**	**25.4 ± 1.6**	**90.0 ± 1.5**	**22.5 ± 1.5**
2	65.2 ± 1.9	40.9 ± 1.9	72.1 ± 1.8	34.0 ± 1.8	64.9 ± 1.9	42.5 ± 1.9	77.3 ± 1.7	28.9 ± 1.7	74.0 ± 1.8	34.5 ± 1.8	**86.7 ± 1.6**	**26.0 ± 1.6**	**89.6 ± 1.5**	**23.6 ± 1.5**
3	61.5 ± 1.9	40.0 ± 1.8	71.3 ± 1.8	35.5 ± 1.8	65.3 ± 1.9	39.4 ± 1.9	77.3 ± 1.7	28.0 ± 1.7	74.1 ± 1.8	33.0 ± 1.8	**86.3 ± 1.6**	**26.5 ± 1.6**	**89.2 ± 1.5**	**24.0 ± 1.5**
4	60.1 ± 1.9	41.5 ± 1.9	71.3 ± 1.8	34.8 ± 1.8	66.4 ± 1.9	40.4 ± 1.9	76.9 ± 1.7	28.5 ± 1.7	73.6 ± 1.8	33.6 ± 1.8	**85.1 ± 1.6**	**26.6 ± 1.6**	**89.5 ± 1.5**	**24.1 ± 1.5**
5	64.4 ± 1.9	40.9 ± 1.9	72.5 ± 1.7	34.6 ± 1.8	63.3 ± 1.8	41.3 ± 1.8	76.2 ± 1.7	27.0 ± 1.7	74.7 ± 1.7	32.8 ± 1.7	**87.2 ± 1.6**	**26.9 ± 1.6**	**88.9 ± 1.5**	**24.5 ± 1.5**
6	62.3 ± 1.9	40.7 ± 1.9	72.2 ± 1.8	34.1 ± 1.8	65.1 ± 1.9	39.7 ± 1.9	78.7 ± 1.7	27.8 ± 1.7	73.9 ± 1.8	32.4 ± 1.8	**86.7 ± 1.6**	**25.9 ± 1.6**	**89.5 ± 1.6**	**24.6 ± 1.5**
7	63.8 ± 1.8	40.1 ± 1.9	72.3 ± 1.8	34.2 ± 1.8	68.1 ± 1.9	38.0 ± 1.9	77.2 ± 1.7	26.2 ± 1.7	74.5 ± 1.8	32.5 ± 1.8	**86.0 ± 1.6**	**25.6 ± 1.6**	**89.7 ± 1.5**	**24.3 ± 1.5**
8	62.6 ± 1.9	40.1 ± 1.9	71.6 ± 1.8	34.6 ± 1.8	66.6 ± 1.9	38.4 ± 1.9	77.4 ± 1.7	26.3 ± 1.7	73.6 ± 1.8	32.0 ± 1.8	**85.9 ± 1.6**	**26.6 ± 1.6**	**89.4 ± 1.5**	**24.4 ± 1.5**
9	61.2 ± 1.9	41.7 ± 1.9	68.9 ± 1.8	33.0 ± 1.8	68.2 ± 1.9	39.5 ± 1.9	78.6 ± 1.7	25.6 ± 1.7	74.5 ± 1.8	32.0 ± 1.8	**85.2 ± 1.6**	**26.9 ± 1.6**	**89.6 ± 1.5**	**24.1 ± 1.5**
10	62.4 ± 1.8	40.3 ± 1.8	70.7 ± 1.8	33.9 ± 1.8	66.5 ± 1.8	38.4 ± 1.9	77.2 ± 1.6	25.8 ± 1.7	72.6 ± 1.7	32.9 ± 1.7	**86.7 ± 1.5**	**26.7 ± 1.6**	**89.4 ± 1.5**	**24.3 ± 1.5**
11	61.8 ± 1.9	41.1 ± 1.9	72.4 ± 1.8	33.8 ± 1.8	68.2 ± 1.9	38.5 ± 1.9	77.6 ± 1.7	25.4 ± 1.7	74.8 ± 1.8	32.5 ± 1.8	**87.0 ± 1.6**	**26.9 ± 1.6**	**90.7 ± 1.5**	**24.1 ± 1.5**
12	64.2 ± 1.9	40.6 ± 1.9	71.3 ± 1.8	34.5 ± 1.8	62.1 ± 1.9	42.6 ± 1.9	78.0 ± 1.7	24.6 ± 1.7	73.5 ± 1.8	32.5 ± 1.8	**86.6 ± 1.6**	**26.4 ± 1.6**	**90.4 ± 1.5**	**24.6 ± 1.5**
13	61.1 ± 1.9	41.9 ± 1.9	70.3 ± 1.8	33.0 ± 1.8	66.3 ± 1.9	40.4 ± 1.9	77.1 ± 1.7	25.0 ± 1.7	73.2 ± 1.8	32.6 ± 1.8	**86.7 ± 1.6**	**26.5 ± 1.6**	**89.6 ± 1.5**	**24.5 ± 1.5**
14	62.2 ± 1.9	41.7 ± 1.9	72.5 ± 1.8	33.2 ± 1.8	68.3 ± 1.9	39.6 ± 1.9	77.6 ± 1.7	25.7 ± 1.7	74.9 ± 1.8	32.4 ± 1.8	**86.4 ± 1.6**	**26.1 ± 1.6**	**89.8 ± 1.5**	**24.0 ± 1.5**
15	61.2 ± 1.9	41.2 ± 1.9	71.4 ± 1.8	33.5 ± 1.8	68.0 ± 1.9	38.3 ± 1.9	77.0 ± 1.7	25.8 ± 1.7	73.7 ± 1.8	32.1 ± 1.8	**87.2 ± 1.6**	**26.0 ± 1.6**	**90.1 ± 1.5**	**24.7 ± 1.5**
16	65.2 ± 1.9	40.7 ± 1.9	72.4 ± 1.8	33.4 ± 1.8	63.1 ± 1.9	41.2 ± 1.9	78.0 ± 1.7	25.6 ± 1.7	74.8 ± 1.8	32.4 ± 1.8	**86.1 ± 1.6**	**26.7 ± 1.6**	**89.4 ± 1.5**	**24.9 ± 1.5**
17	63.3 ± 1.9	40.6 ± 1.9	68.9 ± 1.8	34.2 ± 1.8	67.9 ± 1.9	39.0 ± 1.9	76.3 ± 1.7	25.0 ± 1.7	74.6 ± 1.8	32.0 ± 1.8	**86.4 ± 1.6**	**26.1 ± 1.6**	**89.3 ± 1.5**	**24.2 ± 1.5**
18	68.8 ± 1.9	40.2 ± 1.9	72.1 ± 1.8	34.2 ± 1.8	61.2 ± 1.9	41.3 ± 1.8	77.4 ± 1.7	25.8 ± 1.7	73.0 ± 1.8	32.3 ± 1.8	**85.2 ± 1.6**	**26.5 ± 1.6**	**89.5 ± 1.5**	**24.6 ± 1.5**
	63.0 ± 1.8	40.8 ± 1.8	71.4 ± 1.8	34.0 ± 1.8	65.9 ± 1.8	39.9 ± 1.8	77.5 ± 1.7	26.4 ± 1.7	73.9 ± 1.8	32.5 ± 1.8	86.3 ± 1.6	26.3 ± 1.6	89.6 ± 1.5	24.2 ± 1.5

signal. Therefore, the correlation coefficient is increased by 3.21% for the overall fusion algorithm estimated force ($\hat{Y}_{OF}$).

Many studies had attempted to achieve sEMG–torque and force estimation [23–25], by narrowing it down to a least squares and maximum likelihood estimation problem. These studies report that the sEMG–torque and force estimation failed because of the crosstalk and the sEMG signal noise. From Tables 3 and 4, the fusion algorithm estimated force shows a marked improvement over the individual model estimated force. Therefore the sensor data fusion is reducing the redundancy caused due to cross talk in the skeletal muscle force estimation. As this study is based on the sEMG data, the quantification of the reduced crosstalk is not possible. In [29] the EMG–Force estimation was achieved by using Principle Component Analysis (PCA) and Independent Component Analysis (ICA) on mono-polar high density EMG signals acquired from triceps brachii muscles and the extension force of the elbow. PCA is giving 40% reduction in Root Mean Square Difference between predicted and measured force. In this present work we are not dealing with the sEMG from the triceps, but this work can be extended to any muscle group. The hybrid (combination of WH and SPAFDR) fusion estimation is yielding a 96% mean correlation and a 3.9% mean relative error with a standard deviation of ±1.3 and 0.9 respectively between the estimated and the actual force for 18 test subjects.

In [32], VWA and DKF based data fusion algorithms were implemented and tested on five volunteers. The results were compared

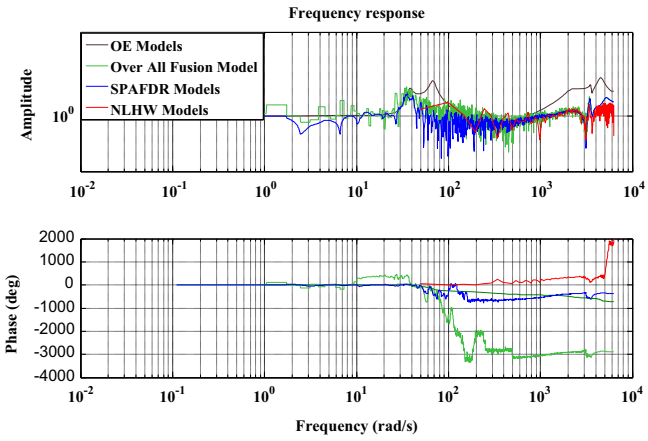

Fig. 10. Frequency Response of OE, WH and SPAFDR Models.

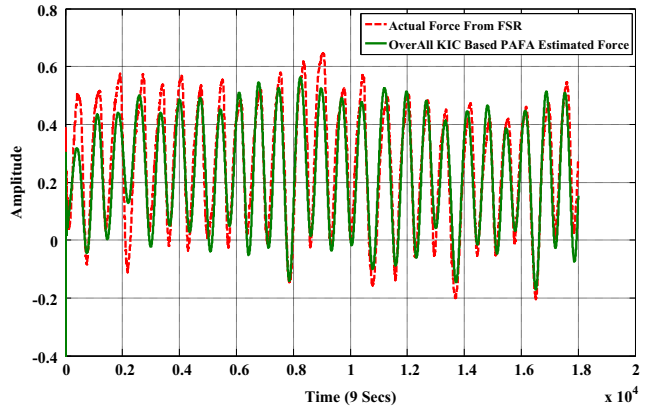

Fig. 11. PAFA estimated force and the actual force plotted together for WH and SPAFDR models during a random grasping action and the X-axis represents the number of data points collected for a duration of 9 s.

based on the absolute error. Because of the dynamic nature of the EMG signal and the variability between test subjects, the reporting of the absolute error can lead to false conclusions. Therefore, in this work, the relative error is primarily used for quantitative analysis of the proposed fusion algorithms. The proposed algorithms were tested with the k-fold cross validation data obtained from 18 test subjects, demonstrating a consistent improvement in estimating the skeletal muscle force when compared to the individual model estimated force. Since the literature doesn't seem to be abundant in the data fusion for sEMG signals it is difficult to make an extensive quantitative comparison of the present research with the existing work.

The sEMG based finger force models (linear, nonlinear and spectral) are constructed based on the normal limb sEMG and a force measurement. The limitation of this work is that these models were not tested on amputees. However, the main idea is to extract the dynamic relationship between sEMG and skeletal muscle force. These dynamic models can be mapped to an individual with an amputation that has a variable amount of residual limb musculature, varying levels of atrophy, and an unknown force output by recalibrating the models with the sEMG data from the amputee using an existing limb or standard force models (in case of multiple limb amputation). This design can also be extended to above elbow amputations by approximating the sEMG data from the motor units of the biceps and triceps . In future it will be interesting to look closely at the model structure of the WH and SPAFDR models to account for the different modeling frequencies that were observed in the Bode plots.

This present research is not only confined to bio-medical applications, but also has extensive applications in computational intelligence, machine learning, uncertainty analysis etc. This work can be implemented in real-time as all the commonly available microcontrollers/processors have numerous Analog to Digital Converter (ADC) channels. The idea of acquiring more sEMG signals by utilizing more sensors for the purpose of inferring more information about the finger forces is shown as a valid approach in this work. Hence, utilizing three or more EMG channels is feasible and from the results presented provides an improved estimate.

6. Conclusion

In this paper, five different filters - Butterworth, Chebyshev Type II, Bayesian Exponential, Bayesian Half-Gaussian and wavelet Db 44 were compared for the sEMG and skeletal muscle force data. WT based Db 44 filter provided a percentage correlation of 70% for sEMG /force WH and SPAFDR models when compared with the other four filters. Because of its high computational cost, when compared with the Butterworth and Chebyshev Type II, the proposed wavelet approach may require a high performance micro-processor/controller for real-time implementation which may be a topic for the future work. In the authors' previous work [19,20,46], linear Output Error (OE) models were investigated. In this work the System Identification (SI) technique is utilized to model the dynamic relationship between sEMG-Force by employing nonlinear Wiener Hammerstein and spectral models. The comparison between the estimated force output and actual force output was made based on the percentage Pearson correlation coefficient and percentage relative error.

Time domain linear OE, nonlinear WH and frequency domain SPAFDR modeling techniques are utilized to analyze the dynamics and the frequency content of the sEMG/skeletal muscle force data from the three sensors. Although better individual models can be inferred using SI under perfect conditions, the fusion algorithms improve the predicted force estimate consistently. The fusion algorithms results were consistent for all the test subjects. The results indicate that the OLMFA is suitable for linear models and the KIC is suitable for nonlinear models. KIC based Nonlinear WH models give 92.7% correlation with a standard deviation of ± 1.4; SPAFRD, 89.6% correlation with a standard deviation of ± 1.5% on average; and the hybrid (combination of the WH and SPAFDR) fusion is yielding 96% mean correlation and 3.9% mean relative error with a standard deviation of ± 1.3 and ± 0.9 respectively between the overall hybrid fusion algorithm estimated and the actual force for 18 test subjects. As an extension this work can be applied to other types of array sensor systems. Therefore this work enhances the current understanding of the relationship between the sEMG and force, and also the sEMG and motor unit activation through direct force recording from the appropriate motor points.

7. Summary

Acquiring and estimating skeletal muscle (hand/finger) forces using surface Electromyography (sEMG) signals is a challenging task due to cross-talk, noise, and temporally and spatially modulated signal characteristics. In general, the sEMG measurements are based on single sensor data. In this paper, an array of sEMG sensors are used and new hybrid fusion techniques are proposed for the estimation of the skeletal muscle force using linear, nonlinear and spectral models. The sEMG signals are pre-processed using Butterworth, Chebyshev Type-II, Exponential, Half-Gaussian and Wavelet transforms. Using a system identification technique, Wiener Hammerstein (WH) models and spectral models are extracted.

A detailed comparison is made for 18 different test subjects, based on Pearson's correlation coefficients and the relative error provided between the filters, the different models, and the hybrid

model using the proposed fusion techniques. The Half-Gaussian (HG) filter is giving 67.7% mean correlation and 35.5% mean relative error with a standard deviatioin of ± 2.5 and ± 2.8 respectively. The Wavelet Transform (WT) based Daubechies 44 (Db) filter at 8 levels of decomposition is giving 72.6% mean correlation and 32.4% mean relative error with a standard deviation of ± 1.7 and ± 1.6 respectively for the sensor that is placed closest to the motor point. It is evident that wavelet transforms are resulting in better performance compared to the other four filters.

Similarly, a comparison is made between the linear, non-linear and spectral models based on the mean percentage Pearson's correlation coefficient and the mean percentage relative error. Non-linear Wiener Hammerstein models with 1-dimensional polynomial non-linearity class are yielding the best performance in modeling the dynamics of the sEMG and skeletal muscle force, i.e. this approach is giving 74.5% mean correlation and 37.2% mean relative error with a standard deviation of ± 1.8 respectively. The spectral models are giving 72.5% mean correlation and 33.2% mean relative error with a standard deviation of ± 1.8 respectively. Two fusion algorithms are proposed and compared. One is the Probability Analysis based Fusion Algorithm (PAFA) and the other is Optimized Linear Model Fusion Algorithm (OLMFA). OLMFA yields better correlation for SPAFDR models. It is clear from Table V that the KIC based PAFA works best for both WH and SPAFDR models. Experimental verification of the fusion based hybrid models with wavelet transform shows a 96% mean correlation and 3.9% mean relative error with a standard deviation of ± 1.3 and ± 0.9 respectively between the overall hybrid fusion algorithm estimated and the actual force for 18 test subjects.

Conflict of interest

None declared.

Acknowledgments

This research was sponsored by the U.S. Department of the Army, under the Award number w81xwh-10-1-0128 awarded and administered by the U.S. Army Medical Research Acquisition Activity, 820 Chandler Street, Fort Detrick, MD 21702-5014. The information does not necessarily reflect the position or the policy of the government, and no official endorsement should be inferred. For the purposes of this article, information includes news releases, articles, manuscripts, brochures, advertisements, still and motion pictures, speeches, trade association proceedings, etc. Further, the help from Dr. Haydie Lecorbeiller in proof reading the manuscript is greatly appreciated. Finally the authors appreciate very much the detailed comments from the reviewers which enhanced the quality of the manuscript.

Appendix

The Pearson correlation coefficient is given by,

$$\rho_{X,Y} = \mathrm{corr}(X,Y) = \frac{\mathrm{cov}(X,Y)}{\sigma_X \sigma_Y} = \frac{E[(X-\mu_X)(Y-\mu_Y)}{\sigma_X \sigma_Y},$$

where X, Y, are random variables, μ_X and μ_Y are expected values, σ_X, σ_y are standard deviations respectively. E is the expected value operator.

The OLMFA resulting MISO transfer function $H(z)$is constructed as follows:

From u_1 to output,

$$\frac{z^8-3.84z^7+7.72z^6-10.78z^5+10.69z^4-7.41z^3+3.60z^2-0.97z+0.11}{z^8-4.02z^7+6.32z^6-4.12z^5-1.54z^4+5.87z^3-5.43z^2+2.28z-0.34}$$

From u_2 to output,

$$\frac{z^8-4.33z^7+9.00z^6-12.42z^5+12.22z^4-8.11z^3+3.42z^2-0.91z+0.14}{z^8-4.02z^7+6.32z^6-4.12z^5-1.54z^4+5.87z^3-5.43z^2+2.28z-0.34}$$

From u_3 to output,

$$\frac{z^8-3.52z^7+6.65z^6-8.86z^5+8.18z^4-5.36z^3+2.42z^2-0.55z+0.09}{z^8-4.02z^7+6.32z^6-4.12z^5-1.54z^4+5.87z^3-5.43z^2+2.28z-0.34}$$

References

[1] Amputee Coalition of America (ACA), National Limb Loss Information Center (NLLIC), Limb Loss Facts in the United States.
[2] E.F. Murphy, A.B. Wilson, Limb prosthetics and orthotics, in: M. Clynes, J. H. Milsum (Eds.), Biomedical Engineering Systems, McGraw-Hill, New York, NY, 1970, pp. 489–549.
[3] C. Potluri, M. Anugolu, Y. Yihun, P. Kumar, S. Chiu, M.P. Schoen, D.S. Naidu, Implementation of sEMG-based real-time embedded adaptive finger force control for a prosthetic hand, in: Proceedings of the IEEE Conference on Decision and Control and European Control Conference, Orlando, Florida, USA, 12–15 December 2011.
[4] M. Zinn, B. Roth, O. Khatib, J.K. Salisbury, A new actuation approach for human friendly robot design, Int. J. Robotic Res. 23 (4–5) (2004) 379–398.
[5] J. Heinzmann, J. Zelinsky, A safe-control paradigm for human-robot interaction, J. Intelligent Robotic Syst. 25 (4) (1999) 295–310.
[6] R. Mereletti, P.A. Parker, Electromyography: Physiology, Engineering and Noninvasive Applications, John Willey & Sons, New Jersey, 2004.
[7] M.B.I. Raez, M.S. Hussain, F. Mohd-Yasin, Techniques of EMG signal analysis: detection, processing, classification and application, Biol. Proced. Online 8 (2006) 11–35.
[8] L.P. Ince, M.S. Leon, D. Christidis, EMG biofeedback with upper extremity musculation for relaxation training: a critical review of the literature, J. Behav. Ther. Exp. Psychiatry. 16 (2) (1985) 133–137.
[9] J.P. Clarya, J. Cabri, Electromyography and the study of sports movements: a review, J. Sports Sci. 11 (No.5) (1993) 379–448.
[10] J. Harlaar, R.A. Redmeijer, P. Tump, R. Peters, E. Hautus, The SYBAR system: integrated recording and display of video, EMG, and force plate data, Behav. Res. Methods Instrum. Comput. 32 (1) (2000) 11–16.
[11] J.R. Cram, G.S. Kasman, J Holtz, Introduction to Surface Electromyography, Aspen Publisher Inc, Gaithersburg, Maryland, 1998.
[12] L. Arendt-Nielsen, K.R. Mills, The relationship between mean power frequency of the EMG spectrum and muscle fiber conduction velocity, Electroencephalogr. Clin. Neurophysiol. 60 (1985) 130–134.
[13] R. Merletti, M. Knaflitz, C.J. De Luca, Myoelectric manifestations of fatigue in voluntary and electrically elicited contractions, J. Appl. Physiol. 69 (1990) 1810–1820.
[14] P. Konrad, The ABC of EMG, A Practical Introduction to Kinesiological Electromyography, Version 1.4, March 2006.
[15] Y. Chen, M. Akutagawa, T. Emoto, Y. Kinouchi, The removal of EMG in EEG by neural networks, IOP Publishing (2010) 1567–1584. (Physiology Measurement).
[16] E.R. Kandel, J.H. Scartz, Principles of Neural Science, Elsevier, North-Holand, New York, 1981.
[17] C.J. De Luca, L. Donald Gilmore, M. Kuznetsov, S.H. Roy, Filtering the surface EMG signal: Movement artifact baseline noise contamination, J. Biomech. 43 (2010) 1573–1579.
[18] T.D. Sanger, Bayesian filtering of myoelectric signals, J. Neurophysiol. 97 (2007) 1839–1845.
[19] C. Potluri, P. Kumar, M. Anugolu, A. Urfer, S. Chiu, D.S. Naidu, M.P. Schoen, Frequency domain surface EMG sensor fusion for estimating finger forces, in: Proceedings of the 32nd Annual International Conference of the IEEE EMBS, Buenos Aires, Argentina, August 31–September 4 2010.
[20] M. Anugolu, A. Sebastian, P. Kumar, M.P. Schoen, A. Urfer, D.S. Naidu, Surface EMG array sensor based model fusion using bayesian approaches for prosthetic hands, in: Proceedings of the Dynamic Systems and Control Conference (DSCC), Hollywood, CA, 2009.
[21] D. Staudenmann, K. Roeleveld, D.F. Stegeman, J.H. Vain Dieen, Review: methodological aspects of SEMG recording for force estimation–a tutorial and review, J. Electromyogr. Kinesiology 20 (2010) 375–387.
[22] J. Hashemi, K. Hashtrudi-Zaad, E. Morin, P. Mousavi, Dynamic modeling of EMG-force relationship using parallel cascade Identification, in: Proceedings of the 32nd Annual International Conference of the IEEE EMBS, Buenos Aires, Argentina, August 31–September 4 2010.
[23] R. Istenic, A. Holobar, R. Merletti, D. Zazula, EMG based muscle force estimation using motor unit twitch model and convolution Kernel Compensation, in: Proceedings of the 11th Mediterranean Conference on Medical and Biomedical Engineering and Computers, IFMBE Proceedings, vol. 16, 2007, pp. 114–117.
[24] F. Mobasser, K. Hashtrudi-Zaad, Rowing stroke force estimation with EMG Signal using artificial neural networks, in: Proceedings of the IEEE Conference on Control Applications, 2005, pp. 825–830.
[25] E.A. Clancy, N. Hogan, Relating agonist-antagonist electromyograms to joint torque during isometric, quasi-isotonic, non fatiguing contractions, IEEE Trans. Biomed. Eng. 44 (10) (1997) 1024–1028.

[26] P.J. Lago, N.B. Jones, Parameter estimation of system dynamics with modulation-type noise-application to the modeling of the dynamic relationship between the EMG and force transients in muscle, IEEE Proc. D Control Theory Appl. 131 (6) (1984) 221–228.
[27] A.R. Luis, N.D. Guilherme, A. Power Wheelchair controlled using hand gestures, a single sEMG sensor, and guided under-determined source signal separation, in: Proceedings of the 4th IEEE RAS/EMBS International Conference on Biomedical Robotics and Biomechanics, Roma, Italy, 24–27 June 2012.
[28] S.J. Sanjay, S.W. Anthony, P.M. Claudi, W. Scott, Brain–muscle–computer interface using a single surface electromyographic signal: initial results, in: Proceedings of the IEEE EMBS Conference on Neural Engineering, Cancun, Mexico, April 27–May 1 2011.
[29] D. Staudenmann, I. Kingma, A. Daffertshofer, D.F. Stegeman, J.H. Van Dieen, Improving EMG-based muscle force estimation by using a high-density EMG grid and principal component analysis, IEEE Trans. Biomed. Eng. 53 (No. 4) (2006) 712–719.
[30] R. Merletti, L. Lo Conte, E. Avignone, P. Guglielminotti, Modeling of surface myoelectric signals I. Model implementation, IEEE Trans. Biomed. Eng. 46 (7) (1999) 810–820.
[31] C. Potluri, P. Kumar, M. Anugolu, A. Urfer, S. Chiu, D.S. Naidu, M.P. Schoen, Frequency domain surface EMG sensor fusion for estimating finger forces, in: Proceedings of the 32nd Annual International Conference of the IEEE EMBS, Buenos Aires, Argentina, August 31–September 4 2010.
[32] N.M. Lopez, F. di Sciasci, C.M. Soria, M.E. Valentinuzzi, Robust EMG sensing system based on data fusion for myoelectric control of a robotic arm, Biomed. Eng. (2009). (Online).
[33] ⟨http://www.isek-online.org/standards_emg.html⟩.
[34] ⟨http://www.delsys.com/Products/Bagnoli_Desktop.html⟩.
[35] ⟨http://www.trossenrobotics.com/productdocs/2010-10-26-Data Sheet-FSR402-Layout2.pdf⟩.
[36] J. Rafiee, M.A. Rafiee, N. Prause, M.P. Schoen, Wavelet basis functions in biomedical signal processing, Expert Syst. Appl. 38 (2010) 6190–6201.
[37] L. Arendt-Nielsen, K.R. Mills, The relationship between mean power frequency of the EMG spectrum and muscle fiber conduction velocity, Electroencephalogr. Clin. Neurophysiol. 60 (1985) 130–134.
[38] M. Abd-Krim Seghouane, G. Bekara, Fluery, A small Sample Model Selection Criterion based on Kullback's Symmetric Divergence, IEEE Trans. Signal Process. 52 (2004) 145–148.
[39] A.R. Liddle, Information Criteria for Astrophysical Model Selection, Astro-ph/071113, pp.1–5, 2008.
[40] H. Chen, S. Huang, A comparative study on model selection and multiple model fusion, in: Proceedings of the 7th International Conference on Information Fusion, 2005, pp.820–826.
[41] S. Konishi, G. Kitagawa, Information Criteria and Statistical Modeling, Springer Ser. Stat. (2008).
[42] C. Potluri, M. Anugolu, S. Chiu, A. Urfer, M. P. Schoen, D. S. Naidu, Fusion of spectral models for dynamic modeling of sEMG and skeletal muscle force, in: Proceedings of the 34th Annual International Conference of the IEEE EMBS, San Diego, CA, USA, August 28–September 1 2012.
[43] M.P. Schoen, Application of Genetic Algorithms to Observe Kalman Filter Identification, J. Vib. Control 14 (No.7) (2008) 971–997.
[44] M.P. Schoen and A. Mahajan, Input Design for the system identification (IDSI) of a ultrasonic 3D position estimation system, in: Proceedings of ASME Winter Meeting, Nashville, Tennessee, 1999, pp. 765–770.
[45] M.P. Schoen, Input design for on-line system identification of a human respiratory system, in: Proceedings of American Control Conference, Anchorage, AK, May 8–10 2002.
[46] J.T. Bingham, M.P. Schoen, Characterization of myoelectric signals using system identification techniques, in: Proceedings of IMECE, Anaheim, California, November 13–19 2004.

Chandrasekhar Potluri received his B.E. in Electronic and Instrumentation Engineering from Andhra University, Andhra Pradesh, India, in 2009, M.S. in Measurement and Control System Engineering from Idaho State University (ISU), Pocatello, Idaho in 2010, Ph.D. in Engineering and Applied Science from ISU in 2013.

Dr. Potluri is working as a Power-train Hardware in the Loop (HIL) Development Engineer at Mercedes-Benz Technology (MBtech-NA) and also he worked as an Adjunct Faculty in the Department of Electrical Engineering at Idaho State University from 2012 to 2013. He worked as a lead Doctoral Research Assistant in Smart Prosthetic Hand Development Project, at Measurement and Control Engineering Research Center (MCERC), ISU, funded by the Telemedicine & Advanced Technology Research Center (TATRC) of the United States Army Medical Research and Material Command (USAMRMC) from 2010 to 2012. Dr. Potluri made significant contributions in sEMG data processing, fusion algorithms and sEMG based real-time acquisition and control of Prostheses. He has more than 27 publications which includes journals and international conferences (to date) in these fields. He is an active member of the IEEE, IFAC and ISA. Dr. Potluri is the recipient of ISU 2012 Outstanding Doctoral Student Award and the 2013 ISU Academic Excellence Award, the highest honors for a graduate student at ISU. He also received a Graduate Research Fellowship for Dynamic Risk Estimation Algorithm Development to Substitute the FMEA Analysis from ON Semiconductor and Mercedes Benz Technology (MBtech-NA) at ISU.

Madhavi Anugolu received her B.E. in Electronics and Instrumentation Engineering from Acharya Nagarjuna University, Andhra Pradesh, India in 2004, M.S. in Measurement and Control Engineering from Idaho State University (ISU), in 2010. She is currently a Ph.D. candidate in Engineering and Applied Science at ISU. She worked as Graduate Research Assistant at Measurement and Control Engineering Research Center (MCERC) in the Smart Prosthetic Hand Development Project funded by the US Department of Defense from 2007 to 2012. She has 14 publications till date. She is working as a Graduate Teaching Assistant for the School of Engineering at ISU. She is also externaly serving as a reviewer for several journals and international conferences. She is the recipient of Associated Students of Idaho State University Scholarship in 2011. Her research interests include Uncertainty Analysis, Data Fusion, Smart Prostheses, Artificial Intelligence and Machine Learning.

Marco P. Schoen was born in 1965 and received his B.S. degree in Mechanical Engineering from the Swiss College of Engineering in 1989, his M.E degree in Mechanical Engineering from Widener University in 1993, and his Ph.D. in Engineering Mechanics from Old Dominion University in 1997. From 1997 to 1998 he was a faculty member at Lake Superior State University and from 1998 to 2001 he served as a faculty to the Mechanical Engineering program at Indian Institute of Technology. Since 2001 he has been with Idaho State University, where he is currently serving as professor and the chair for the Department of Mechanical Engineering and as associate director for the Measurement and Control Engineering Research Center (MCERC). His research addresses topics in controls and vibration of biomedical and aerospace systems as well as energy related problems. Schoen has been an associate and a past chair of the Model Identification and Intelligent Systems (MIIS) Technical Committee for the American Society of Mechanical Engineers (ASME).

D. Subbaram Naidu received his B.E. degree in Electrical Engineering from Sri Venkateswara University, Tirupathi, Andhra Pradesh, M.Tech. degree in Control System Engineering and Ph.D. degree in Electrical Engineering from Indian Institute of Technology (IIT) Kharagpur, India.

Dr. Naidu worked at NASA Langley Research Center, US Air force Research Laboratory, Norwegian University of Science and Technology, Swiss Federal Institute of Technology, Universities of Southern and Western Australia. Since 1990, he has been with Idaho State University where he is Professor and Director of School of Engineering and for the Measurement and Control Engineering Research Center (MCERC). Dr. Naidu has over 200 publications including 6 books. He has been a member of several editorial boards of professional journals. He is an elected IEEE Fellow since 1995.

Alexander G. Urfer, PT, Ph.D., is currently Adjunct Professor of Physical Therapy and Physiology at Idaho State University in the department of Physical and Occupational Therapy. He received his BA in Health Education from Montclair State University in 1972, his MA and Ph.D. in Human Physiology from the Ohio State University in 1977 and a Certificate in Physical therapy from Mayo Clinic in 1990. He has served in the capacity of a full time faculty member in Biology from 1977 to 1990 and a Professor of Physical Therapy and Physiology, as well as Department Chair in Physical Therapy, from 1990 to 2009. Dr. Urfer teaches in the areas of Biomechanics, Orthopedics and has research interests in Prosthetics, Orthopedics, Clinical Physical Therapy, and Therapeutic Exercise. He is a member of the American Physical Therapy Association. He has been a manuscript reviewer of the Journal of Orthopedic and Sports Physical Therapy and past President of the North West Chapter of the American College of Sports Medicine.

Steve C. **Chiu** (M'96) is an Associate Professor of Electrical Engineering at Idaho State University. He also holds an appointment as Associate Professor in Residence with the Computer Science and Engineering Department at the University of Connecticut. Dr. Chiu received his Ph.D. in Electrical and Computer Engineering from Northwestern University in 2004, an M.S. in Engineering Management from Northwestern University in 1995, and a B.S. in Electrical Engineering from University of Illinois at Chicago in 1990.

Prior to his current appointments, Dr. Chiu worked in certification and telecommunication industries as a project and R&D engineer. Steve was a referee for several publications in computer science and engineering, including CISE, JPDC, FGCS, and LNCS, and serves on the editorial review board of the IJHCR as well as a Guest Editor for the JSUPE. His academic honors include a Ph.D. research assistantship award, a post-doctoral research associate award, a best research poster award, as well as several professional citations. Dr. Chiu is a member of the IEEE and its Technical Committee on TCPP. He is also a member of the Tau Beta Pi Engineering Honor Society.